

Resonant single leptoquark production at hadron colliders

Luca Buonocore,^{1,2,*} Ulrich Haisch,^{3,†} Paolo Nason,^{4,‡} Francesco Tramontano,^{1,§} and Giulia Zanderighi^{3,¶}

¹*Dipartimento di Fisica, Università di Napoli Federico II and INFN, Sezione di Napoli, I-80126 Napoli, Italy*

²*Physik Institut, Universität Zürich, CH-8057 Zürich, Switzerland*

³*Max-Planck-Institut für Physik, Föhringer Ring 6, 80805 München, Germany*

⁴*Università di Milano-Bicocca and INFN, Sezione di Milano-Bicocca, Piazza della Scienza 3, 20126 Milano, Italy*

A novel strategy to search for leptoquark (LQ) production at the Large Hadron Collider (LHC) is proposed. Our method relies on the observation that the probability to find a charged lepton with a given momentum fraction in the proton (p) is sufficiently large to allow for a measurable rate of s -channel production of a hypothetical LQ in pp collisions. In our analysis, decay final states with a high transverse momentum (p_T) electron or muon and a high- p_T light-flavour jet are targeted. Using the precision calculation of the lepton parton distribution functions that recently became available, we derive, for the case of scalar LQs, new bounds for the different flavour final states that arise from the LHC Run II. These limits represent the most stringent direct constraints to date on minimal first- and second-generation scalar LQs in large parts of the parameter space. The prospects of our method at future LHC runs are also explored.

PACS numbers: 14.80.Sv, 25.30.-c

Introduction. Leptoquarks (LQs) are hypothetical coloured bosons that carry both a baryon number and a lepton number [1], meaning they all have in common that once produced they can decay to a lepton (ℓ) and a quark (q) — see [2] for a recent LQ review. Because of their non-zero colour charge, LQs can be pair-produced at hadron colliders via gluon-fusion (i.e. $gg \rightarrow \text{LQ}\bar{\text{LQ}} \rightarrow (\ell q)(\ell q)$) or quark-fusion (i.e. $q\bar{q} \rightarrow \text{LQ}\bar{\text{LQ}} \rightarrow (\ell q)(\ell q)$). For sufficiently large LQ-lepton-quark couplings, also pair-production via t -channel exchange of a lepton becomes relevant, and LQ exchange contributes to Drell-Yan like dilepton production $q\bar{q} \rightarrow \ell^+\ell^-$ and single LQ production in $gq \rightarrow \ell^+\ell^-q$. Both the ATLAS and CMS collaborations have exploited the different channels at the Large Hadron Collider (LHC) to constrain the parameter space of LQ models (cf. [3–9] for results obtained at a centre-of-mass energy of $\sqrt{s} = 13$ TeV) and the subject has also received renewed theoretical interest (see for instance [10–15]).

In this letter, we present a new search strategy for LQs at hadron colliders, which relies on the fact that once QED interactions are considered, charged-lepton parton distribution functions (PDFs) of the proton (p) are generated. The lepton PDFs are small compared to that of quarks and gluons, since they are suppressed by two powers of the ratio of the electromagnetic coupling constant α_{em} over the strong coupling constant α_s . A first implementation of a PDF set with leptons was put forward in [16], that was however affected by large uncertainties. Based upon the so-called LUX method [17, 18], a precise determination of the lepton PDFs has become available recently [19]. These lepton PDFs have been combined with the NNPDF3.1luxQED set [20] into a new PDF set dubbed LUXlep [19]. In the following we will use the LUXlep set to compute the cross sections for resonant single LQ production $\ell q \rightarrow \text{LQ} \rightarrow \ell q$ in pp collisions, studying final states with a high transverse momentum (p_T) elec-

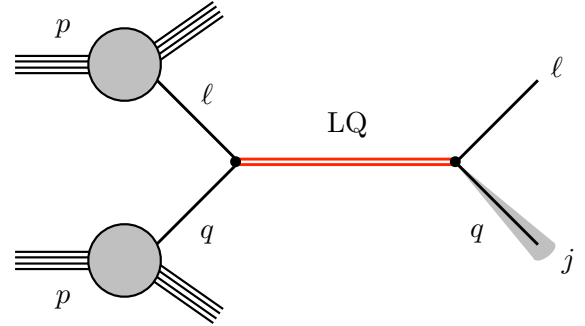


FIG. 1. Tree-level Feynman diagram describing resonant single LQ production in pp collisions with a final state consisting of a lepton and a jet.

tron (e) or muon (μ) and a high- p_T light-flavour jet (j), to derive bounds on the parameter space for the different flavour final states of first- and second-generation scalar LQs. The corresponding tree-level Feynman diagram is shown in Fig. 1.

LQ interactions. We follow [14] and consider scalar LQs which couple only to one lepton and quark flavour, taking them to be singlets under the $SU(2)_L$ part of the Standard Model (SM) gauge group. In order to obtain $SU(2)_L$ invariant interactions, we couple the LQs to the $SU(2)_L$ singlet leptons and quarks, i.e. the right-handed SM fermions. Using the notation where all singlet fields are represented by left-handed charge conjugate fields, the scalar LQ coupling to singlet electrons and up quarks can then be written as

$$\mathcal{L} \supset \lambda_{eu} \text{LQ}_{eu} (E^c U^c)^* + \text{h.c.}, \quad (1)$$

where the spinor indices of E^c and U^c are contracted anti-symmetrically. In the limit of large scalar LQ masses, i.e. $M \gg m_\ell, m_q$, the corresponding total decay width of the LQ is given by

$$\Gamma = \frac{|\lambda_{eu}|^2}{16\pi} M, \quad (2)$$

* Electronic address: luca.buonocore@na.infn.it

† Electronic address: haisch@mpp.mpg.de

‡ Electronic address: paolo.nason@mib.infn.it

§ Electronic address: francesco.tramontano@cern.ch

¶ Electronic address: zanderi@mpp.mpg.de

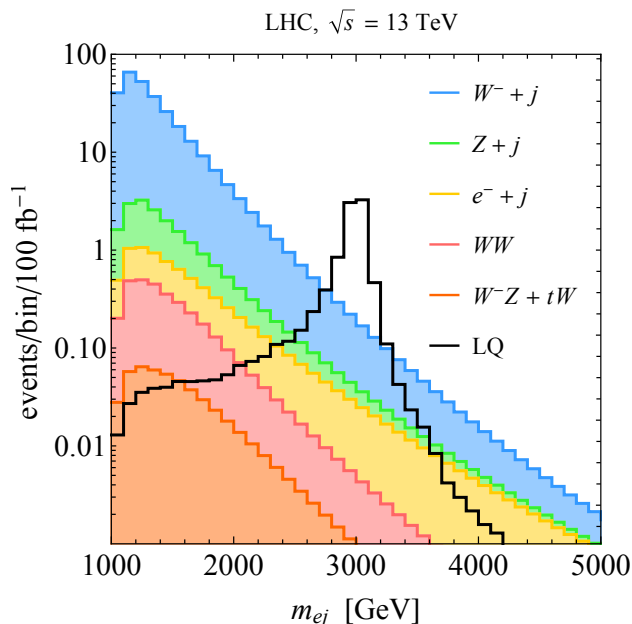


FIG. 2. Distributions of m_{ej} after imposing the experimental selection requirements as detailed in the text. The coloured histograms are stacked and represent the SM backgrounds. The LQ signal prediction corresponds to $M = 3$ TeV and $\lambda_{eu} = 1$ and is superimposed as a black line. The events are binned in 100 GeV bins and all predictions are obtained for 100 fb^{-1} of pp collisions at $\sqrt{s} = 13$ TeV.

and due to the minimal character of the LQ, it decays almost exclusively to the eu final state. The expressions (1) and (2) also apply to all other flavour combinations after obvious replacements of fields and indices.

Analysis strategy. Event generation and showering is performed with `MadGraph5_aMCNLO` [21] and `PYTHIA 8.2` [22]. Since at present `PYTHIA 8.2` cannot handle incoming leptonic partons, we have replaced all initial state leptons by photons in the Les Houches files to shower the events. As a result our simulation does not include leptons but quarks arising from photon splitting in the parton shower backward evolution.¹ The signal predictions corresponding to s -channel single LQ production $pp \rightarrow \text{LQ} \rightarrow \ell q$ are generated at leading order (LO) using the implementation of the Lagrangian (1) presented in [12] together with `LUXlep` PDFs [19].

Our analysis uses experimentally identified jets, electrons, muons and missing transverse energy ($E_{T,\text{miss}}$). `FastJet 3` [24] is used to construct anti- k_t jets [25] of radius $R = 0.4$. Our analysis is implemented in `CheckMATE 2` [26], which employs `Delphes 3` [27] as a fast detector simulator. Detector effects are simulated by smearing the momenta of the reconstructed objects, and by applying reconstruction and identification efficiency factors tuned to mimic the performance of the ATLAS detector. In particular, electron

candidates are required to satisfy the tight identification criteria of ATLAS [28], while muon candidates must fulfil the ATLAS quality selection criteria optimised for high- p_T performance [29, 30]. The corresponding reconstruction and identification efficiency for electrons amounts to 90% for $p_T > 500$ GeV, while for muons the reconstruction and identification efficiency is 69% (57%) at $p_T = 1$ TeV ($p_T = 2.5$ TeV) — cf. for example [31, 32]. $E_{T,\text{miss}}$ is reconstructed from the sum of the smeared calorimeter deposits, including an extra smearing factor that effectively parametrises additional QCD activity due to pile-up and has been tuned to match the ATLAS distributions.

The basic selections in our signal region require a lepton (e or μ) with $|\eta_\ell| < 2.5$ and $p_{T,\ell} > 500$ GeV and a light-flavour jet with $|\eta_j| < 2.5$ and $p_{T,j} > 500$ GeV. We furthermore demand $E_{T,\text{miss}} < 50$ GeV, veto events that contain additional leptons with $|\eta_\ell| < 2.5$ and $p_{T,\ell} > 7$ GeV and impose a jet veto on subleading jets with $|\eta_j| < 2.5$ and $p_{T,j} > 30$ GeV.² The jet veto limits the amount of hadronic activity and ensures that the background from $t\bar{t}$, s - and t -channel single top production are negligible in the signal region.

The dominant SM background turns out to be $W^- + j$ production which is generated at next-to-leading order (NLO). Next-to-next-leading order QCD and electroweak effects that would effectively reduce the size of the $W^- + j$ background prediction in the phase space region of interest [33] are not included in our analysis. Subleading backgrounds arise from $Z + j$, WW , W^-Z and tW production and are simulated at LO and normalised to the known NLO cross sections. At high values of $m_{\ell j}$ also $\ell^- + j$ production from an initial-state lepton and quark via t -channel exchange of a photon or Z boson represents a relevant irreducible background. We include this background at LO.³ For each background process, the number of events after cuts is fitted and extrapolated to high invariant lepton-jet masses $m_{\ell j}$ using $e^{-a} m_{\ell j}^{b+c \ln m_{\ell j}}$. This functional form is commonly used in experimental searches (see for instance [32]).

In Fig. 2 the distributions of the invariant mass m_{ej} of the electron and the leading jet are displayed for the SM backgrounds, and for a benchmark scalar LQ with mass $M = 3$ TeV and $\lambda_{eu} = 1$, after applying the event selection described above. An integrated luminosity of 100 fb^{-1} under LHC Run II conditions is assumed. Our benchmark LQ has a width of $\Gamma \simeq 60$ GeV. One observes that the sum of the SM backgrounds is a steeply falling distribution, while the LQ signal exhibits a narrow peak as indicated by the black line. The $t\bar{t}$, s - and t -channel single top backgrounds are not shown, since they are very small.

Notice that our background prediction does not include fake electrons from jet misidentification and non-prompt electrons from the decay of heavy-flavoured hadrons. In actual experimental analyses the background contributions

¹ We remark that the inclusion of incoming leptons in shower Monte Carlos is not difficult to realise and one can expect it to become available in the near future [23].

² Since we have replaced incoming leptons with photons, the jet- and lepton-veto induce a mismodelling of the signal strength. We estimate this effect to be of $\mathcal{O}(10\%)$, and therefore to only mildly affect the derived LQ limits.

³ As a check of the simulation we have computed the signal and backgrounds also using `POWHEG` [34–40], and modelled detector effects by simple smearing of the particle momenta at the Monte Carlo truth level, along the lines of [19].

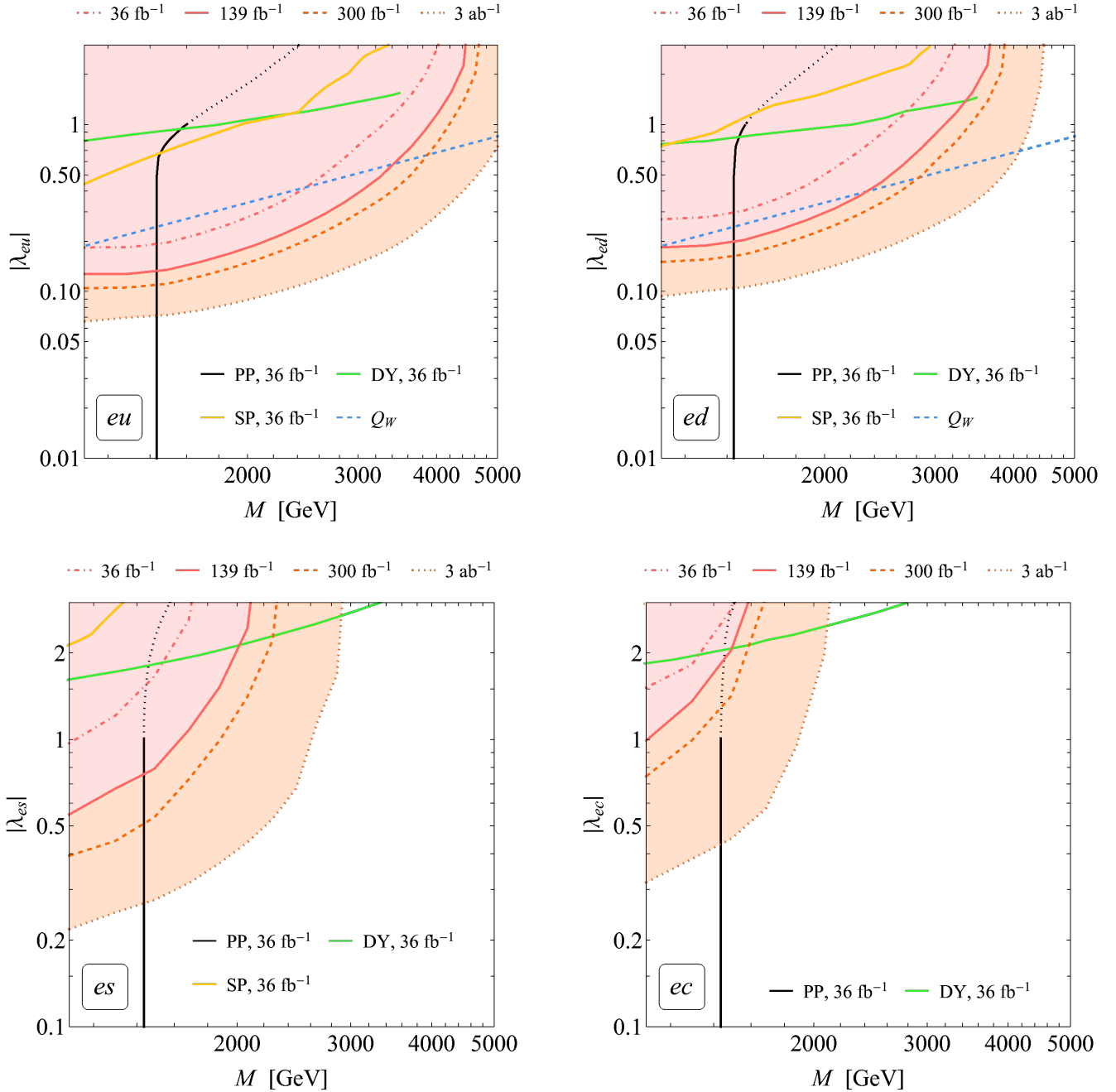


FIG. 3. 95% CL limits on the parameter space of minimal LQ_{eq} bosons with $q = u, d, s, c$. The red (orange) shaded regions correspond to the parameter space that is excluded by resonant single LQ production at the LHC Run II (future LHC runs). The black lines indicate the PP limits obtained in [14] by recasting the results [9], the green lines correspond to the DY bounds derived in [14] using [41], while the yellow lines represent the SP projections [14] of the search [42]. The dashed blue lines correspond to the constraints from Q_W measurements [14]. The parameter spaces to the left and/or above the lines are ruled out. See text for further details.

from events with fake or non-prompt leptons is typically extracted from the data using a matrix method as described for example in [43]. Since we cannot perform such a data-driven background estimate, we mimic the impact of the multijet background in our analysis by incorporating them into the systematic background uncertainties. Specifically, we employ the post-fit systematic uncertainties in the expected number of events for the total background reported

in the recent ATLAS $\ell + E_{T,\text{miss}}$ analysis [32]. Doubling the given errors we find, in the case of electrons, total background uncertainties of 3%, 30% and 250% for m_{e_j} values of 1 TeV, 3 TeV and 5 TeV, respectively. The corresponding numbers in the case of final states with a muon turn out to be 3%, 24% and 50%. The quoted uncertainties will be used below when determining the bounds on the LQ parameter space that can be obtained at the LHC.

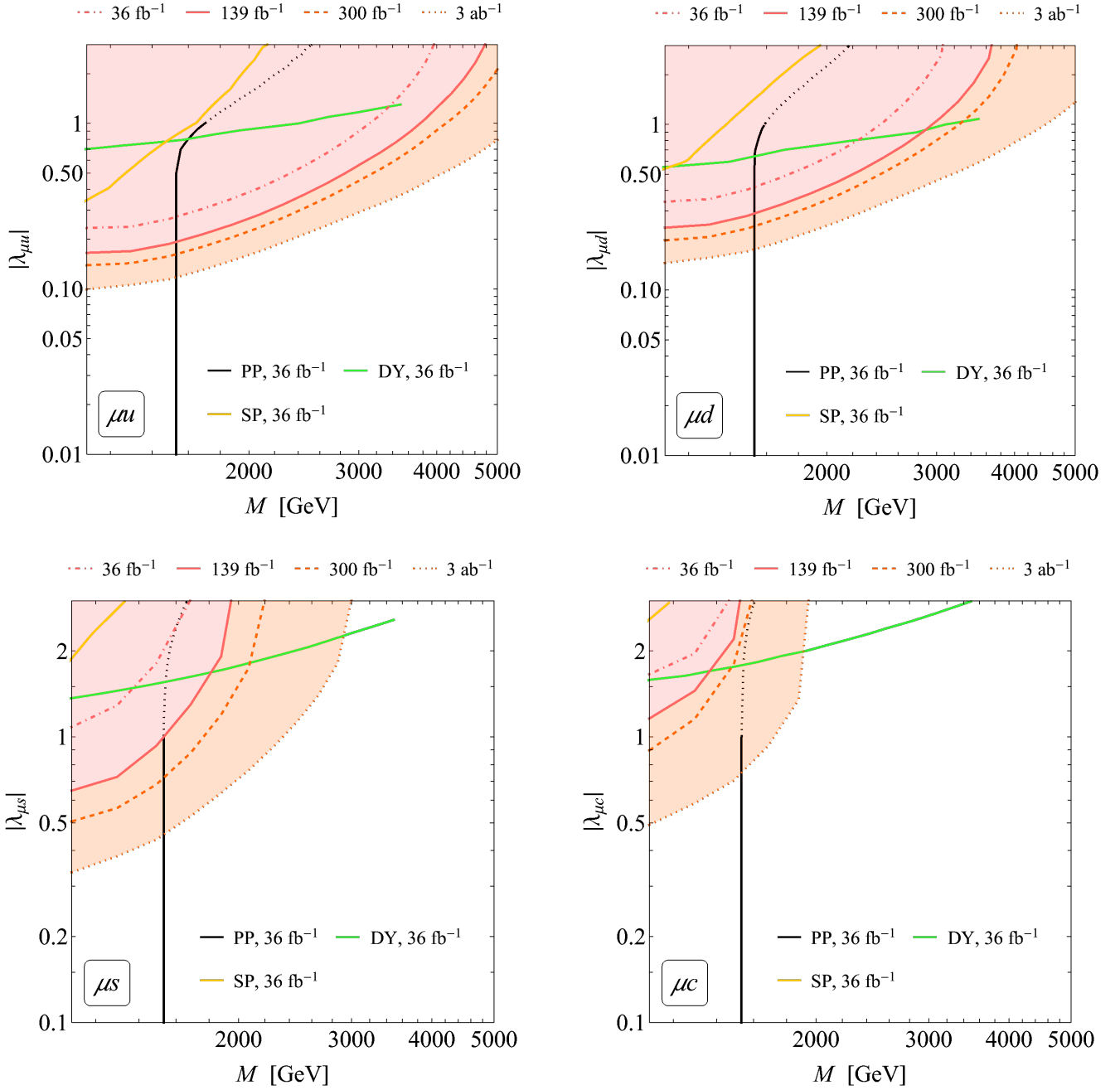


FIG. 4. 95% CL limits on the parameter space of minimal $LQ_{\mu q}$ bosons with $q = u, d, s, c$. Apart from the PP exclusions that have been obtained in [14] by a recast of [7], the colours, styles and meanings of the shown bounds resemble those of Fig. 3. Consult the main text for further explanations.

LHC constraints. The resonance line shape of the LQ signal is modelled by a relativistic Breit-Wigner that is fitted to the distribution of events after showering, reconstruction and cuts. In this way the broadening of the peak by PDF, parton shower and non-perturbative effects is described. We find that the convoluted signal is broader by a factor of 4.2 (2.2) than the initial signal for $M = 2$ TeV ($M = 5$ TeV).

The statistical significance of any localised excess in the $m_{\ell j}$ distribution is quantified using a sliding window approach after binning the background and signal predictions. The bin size is thereby taken to be equal to the $m_{\ell j}$ res-

olution. This resolution is estimated by combining the information on the dilepton and dijet mass resolutions given in [31] and [44], respectively. Using a simple error propagation, we find that the mass resolution amounts to 2.2% (4.3%) at 1 TeV and 1.5% (11%) at 5 TeV in the electron (muon) case. The width of the search window is then varied from a minimum of twice the $m_{\ell j}$ resolution up to 2 TeV, and the optimal width is determined for each signal hypothesis such that the LQ signal deviates most significantly from the smooth background distribution. The significance is calculated as a Poisson ratio of likelihoods modified to in-

corporate systematic uncertainties on the background using the Asimov approximation [45].

Figs. 3 and 4 display the most relevant 95% confidence level (CL) limits on the magnitude of the couplings $\lambda_{\ell q}$ as a function of the mass M for first- and second-generation scalar LQs. The bounds that derive from our novel search strategy for resonant single LQ production are displayed as red (LHC Run II constraints) and orange (projections) shaded regions. The dashed-dotted red, solid red and dashed orange lines assume an integrated luminosity of 36 fb^{-1} , 139 fb^{-1} and 300 fb^{-1} for pp collisions at $\sqrt{s} = 13 \text{ TeV}$, respectively, while the dotted orange lines assume 3 ab^{-1} of $\sqrt{s} = 14 \text{ TeV}$ data. The most stringent limits on the mass of first-generation [9] and second-generation [7] scalar LQs, obtained from pair-production (PP) searches, are indicated as black lines. These limits are based on 36 fb^{-1} of LHC Run II data and correspond to $M > 1435 \text{ GeV}$ and $M > 1530 \text{ GeV}$ for first- and second-generation LQs, respectively. Strictly speaking, they only apply to the case of vanishing LQ-lepton-quark couplings, since PP via t -channel exchange of a lepton has not been considered in the CMS analyses. As shown in [14] this simplification has, however, a minor impact for $|\lambda_{\ell q}| \lesssim 1$. Since the inclusion of lepton exchange diagrams leads to a non-negligible theoretical uncertainty due to missing NLO corrections, following [14] we include the lepton exchange contribution and indicate the PP bounds by dotted black lines for $|\lambda_{\ell q}| > 1$. The green lines correspond to the Drell-Yan (DY) bounds derived in [14] from the CMS results [41], while the yellow lines depict the single production (SP) projections [14] of the CMS LHC Run I search [42]. Both sets of bounds assume 36 fb^{-1} of pp collisions at $\sqrt{s} = 13 \text{ TeV}$. The couplings $\lambda_{e q}$ with $q = u, d$ are also subject to the constraints arising from atomic parity violation, and from parity-violating electron scattering experiments that measure the weak charge (Q_W) of protons and nuclei. The relevant 95% CL bound reads $|\lambda_{e q}| < 0.17 M/\text{TeV}$ [14] and is shown in the upper two panels of Fig. 3 as a dashed blue line. As is evident from these panels, in the case of λ_{eu} (λ_{ed}) the hypothetical 139 fb^{-1} bounds obtained from s -channel single LQ production are more stringent than the constraints from Q_W measurements for $M \lesssim 3.4 \text{ TeV}$ ($M \lesssim 2.3 \text{ TeV}$). In the high-luminosity phase of the LHC (HL-LHC) the corresponding limits can

be expected to surpass the bounds from Q_W measurements for scalar LQ masses up to around 5.2 TeV (4.1 TeV).

Conclusions and outlook. In this letter, we have demonstrated that s -channel single LQ production provides very sensitive direct probes of first- and second-generation scalar LQs at the LHC. Our new proposal takes advantage of the fact that the lepton PDFs in the proton are sufficiently large to yield measurable rates for $\ell q \rightarrow \text{LQ} \rightarrow \ell q$ scattering in pp collisions. By studying final states with a high- p_T electron or muon and a light-flavour jet, we have shown that a simple $E_{T,\text{miss}}$ requirement combined with a lepton and jet veto are sufficient to suppress all relevant SM backgrounds to a level that allows for a successful bump hunt for LQ masses in the TeV range, potentially leading to a discovery. For the case of minimal first- and second-generation scalar LQs, we have performed a dedicated analysis and found that the limits that can be derived from LHC Run II data can represent the most stringent direct constraints to date in large parts of the parameter space. In fact, the obtained exclusions are so strong that they even surpass the indirect limits from Q_W measurements that constrain the LQ- e - u (LQ- e - d) coupling for LQ masses below 3.4 TeV (2.3 TeV). At the HL-LHC the latter bounds can be expected to be pushed up to approximately 5.2 TeV (4.1 TeV). In view of the simplicity of the proposed LQ signature and its discovery reach, we urge the ATLAS and CMS collaborations to perform dedicated resonance searches in final states featuring a single electron or muon and a single light-flavoured jet in future LHC runs.

We finally note that after some modifications the general search strategy proposed by us can also be applied to other flavour combinations and/or other LQ quantum numbers and spins. A particular interesting application in this context seems to be the case of third-generation vector LQs that may be constrained by looking for a resonant signal in the τb channel. Given the more complicated nature of this final state, performing a dedicated analysis is, however, beyond the scope of this letter and thus left for future work.

Acknowledgements. UH thanks Jonas Lindert and Giacomo Polesello for helpful discussions. The research of LB is supported in part by the Swiss National Foundation under contracts 200020_188464 and IZSAZ2_173357. PN acknowledges support from Fondazione Cariplo and Regione Lombardia, grant 2017-2070, and from INFN.

-
- [1] J. C. Pati and A. Salam, *Phys. Rev. D* **10**, 275 (1974), [Erratum: *Phys. Rev. D* **11**, 703–703 (1975)].
 - [2] I. Doršner, S. Fajfer, A. Greljo, J. F. Kamenik, and N. Košnik, *Phys. Rept.* **641**, 1 (2016), [arXiv:1603.04993 \[hep-ph\]](#).
 - [3] M. Aaboud *et al.* (ATLAS), *New J. Phys.* **18**, 093016 (2016), [arXiv:1605.06035 \[hep-ex\]](#).
 - [4] M. Aaboud *et al.* (ATLAS), *Eur. Phys. J.* **C79**, 733 (2019), [arXiv:1902.00377 \[hep-ex\]](#).
 - [5] M. Aaboud *et al.* (ATLAS), *JHEP* **06**, 144, [arXiv:1902.08103 \[hep-ex\]](#).
 - [6] V. Khachatryan *et al.* (CMS), *JHEP* **03**, 077, [arXiv:1612.01190 \[hep-ex\]](#).
 - [7] A. M. Sirunyan *et al.* (CMS), *Phys. Rev.* **D99**, 032014 (2019), [arXiv:1808.05082 \[hep-ex\]](#).
 - [8] A. M. Sirunyan *et al.* (CMS), *JHEP* **03**, 170, [arXiv:1811.00806 \[hep-ex\]](#).
 - [9] A. M. Sirunyan *et al.* (CMS), *Phys. Rev.* **D99**, 052002 (2019), [arXiv:1811.01197 \[hep-ex\]](#).
 - [10] D. A. Faroughy, A. Greljo, and J. F. Kamenik, *Phys. Lett.* **B764**, 126 (2017), [arXiv:1609.07138 \[hep-ph\]](#).
 - [11] B. Diaz, M. Schmaltz, and Y.-M. Zhong, *JHEP* **10**, 097, [arXiv:1706.05033 \[hep-ph\]](#).
 - [12] I. Doršner and A. Greljo, *JHEP* **05**, 126, [arXiv:1801.07641 \[hep-ph\]](#).
 - [13] A. Angelescu, D. Bečirević, D. A. Faroughy, and O. Sumensari, *JHEP* **10**, 183, [arXiv:1808.08179 \[hep-ph\]](#).
 - [14] M. Schmaltz and Y.-M. Zhong, *JHEP* **01**, 132, [arXiv:1810.10017 \[hep-ph\]](#).
 - [15] M. J. Baker, J. Fuentes-Martín, G. Isidori, and M. König,

- Eur. Phys. J. C* **79**, 334 (2019), arXiv:1901.10480 [hep-ph].
- [16] V. Bertone, S. Carrazza, D. Pagani, and M. Zaro, *JHEP* **11**, 194, arXiv:1508.07002 [hep-ph].
- [17] A. Manohar, P. Nason, G. P. Salam, and G. Zanderighi, *Phys. Rev. Lett.* **117**, 242002 (2016), arXiv:1607.04266 [hep-ph].
- [18] A. V. Manohar, P. Nason, G. P. Salam, and G. Zanderighi, *JHEP* **12**, 046, arXiv:1708.01256 [hep-ph].
- [19] L. Buonocore, P. Nason, F. Tramontano, and G. Zanderighi, in preparation (2020).
- [20] V. Bertone, S. Carrazza, N. P. Hartland, and J. Rojo (NNPDF), *SciPost Phys.* **5**, 008 (2018), arXiv:1712.07053 [hep-ph].
- [21] J. Alwall, R. Frederix, S. Frixione, V. Hirschi, F. Maltoni, O. Mattelaer, H. S. Shao, T. Stelzer, P. Torrielli, and M. Zaro, *JHEP* **07**, 079, arXiv:1405.0301 [hep-ph].
- [22] T. Sjöstrand, S. Ask, J. R. Christiansen, R. Corke, N. Desai, P. Ilten, S. Mrenna, S. Prestel, C. O. Rasmussen, and P. Z. Skands, *Comput. Phys. Commun.* **191**, 159 (2015), arXiv:1410.3012 [hep-ph].
- [23] P. Richardson and T. Sjöstrand, private communication.
- [24] M. Cacciari, G. P. Salam, and G. Soyez, *Eur. Phys. J.* **C72**, 1896 (2012), arXiv:1111.6097 [hep-ph].
- [25] M. Cacciari, G. P. Salam, and G. Soyez, *JHEP* **04**, 063, arXiv:0802.1189 [hep-ph].
- [26] D. Dercks, N. Desai, J. S. Kim, K. Rolbiecki, J. Tattersall, and T. Weber, *Comput. Phys. Commun.* **221**, 383 (2017), arXiv:1611.09856 [hep-ph].
- [27] J. de Favereau, C. Delaere, P. Demin, A. Giammanco, V. Lemaître, A. Mertens, and M. Selvaggi (DELPHES 3), *JHEP* **02**, 057, arXiv:1307.6346 [hep-ex].
- [28] G. Aad *et al.* (ATLAS), *JINST* **14** (12), P12006, arXiv:1908.00005 [hep-ex].
- [29] G. Aad *et al.* (ATLAS), *Eur. Phys. J.* **C76**, 292 (2016), arXiv:1603.05598 [hep-ex].
- [30] G. Aad *et al.* (ATLAS), (2020), arXiv:2004.13447 [hep-ex].
- [31] G. Aad *et al.* (ATLAS), *Phys. Lett.* **B796**, 68 (2019), arXiv:1903.06248 [hep-ex].
- [32] G. Aad *et al.* (ATLAS), *Phys. Rev.* **D100**, 052013 (2019), arXiv:1906.05609 [hep-ex].
- [33] J. Lindert *et al.*, *Eur. Phys. J. C* **77**, 829 (2017), arXiv:1705.04664 [hep-ph].
- [34] P. Nason, *JHEP* **11**, 040, arXiv:hep-ph/0409146.
- [35] S. Frixione, P. Nason, and C. Oleari, *JHEP* **11**, 070, arXiv:0709.2092 [hep-ph].
- [36] S. Alioli, P. Nason, C. Oleari, and E. Re, *JHEP* **09**, 111, [Erratum: *JHEP* **02**, 011], arXiv:0907.4076 [hep-ph].
- [37] S. Alioli, P. Nason, C. Oleari, and E. Re, *JHEP* **06**, 043, arXiv:1002.2581 [hep-ph].
- [38] E. Re, *Eur. Phys. J. C* **71**, 1547 (2011), arXiv:1009.2450 [hep-ph].
- [39] S. Alioli, P. Nason, C. Oleari, and E. Re, *JHEP* **01**, 095, arXiv:1009.5594 [hep-ph].
- [40] T. Melia, P. Nason, R. Röntsch, and G. Zanderighi, *JHEP* **11**, 078, arXiv:1107.5051 [hep-ph].
- [41] A. M. Sirunyan *et al.* (CMS), *JHEP* **06**, 120, arXiv:1803.06292 [hep-ex].
- [42] V. Khachatryan *et al.* (CMS), *Phys. Rev. D* **93**, 032005 (2016), [Erratum: *Phys. Rev. D* **95**, 039906 (2017)], arXiv:1509.03750 [hep-ex].
- [43] M. Aaboud *et al.* (ATLAS), *Phys. Lett. B* **762**, 334 (2016), arXiv:1606.03977 [hep-ex].
- [44] G. Aad *et al.* (ATLAS), *JHEP* **03**, 145, arXiv:1910.08447 [hep-ex].
- [45] G. Cowan, *Discovery sensitivity for a counting experiment with background uncertainty* (2012).